

The FMO2 analysis of the ligand-receptor binding energy: the Biscarbene-Gold(I)/DNA G-Quadruplex case study.

Roberto Paciotti^{1,*}, Cecilia Coletti¹, Alessandro Marrone¹, Nazzareno Re¹

¹ Department of Pharmacy, Università “G. D’Annunzio” di Chieti-Pescara, Chieti, Italy

* corresponding to: r.paciotti@unich.it

Keywords:

ab initio calculations, FMO, ligand efficiency, binding energy, biscarbene-Au(I) ligands, DNA G-quadruplex, metal-based drugs

Abbreviation

CADD, computer-assisted drug discovery;
Gq, G-quadruplex;
DNA, deoxyribonucleic acid;
FF, force field;
FE, fragment efficiency;
FMO, fragment molecular orbital method;
FRET, fluorescence resonance energy transfer assay;
F2LE, FMO2 ligand efficiency;
L, ligand;
LR, ligand-receptor complex;
MD, molecular dynamics;
MEP, molecular electrostatic potential;
MM, molecular mechanics
MM/GBSA, molecular mechanics/generalized Born surface area method;
MM/PBSA, molecular mechanics/ Poisson-Boltzmann surface area method;
PIE, pair interaction energy;
PIEDA, pair interaction energy decomposition analysis;
QM, quantum mechanics;
R, receptor.

Abstract

In this work, the *ab initio* fragment molecular orbital (FMO) method was applied to calculate and analyze the binding energy of two biscarbene-Au(I) derivatives, $[\text{Au}(\text{9-methylcaffeine-8-ylidene})_2]^+$ and $[\text{Au}(\text{1,3-dimethylbenzimidazol-2-ylidene})_2]^+$, to the DNA G-Quadruplex structure. The FMO2 binding energy considers the ligand-receptor complex as well as the isolated forms of energy-minimum state of ligand and receptor, providing a better description of ligand-receptor affinity compared with simple pair interaction energies (PIE). Our results highlight important features of the binding process of biscarbene-Au(I) derivatives to DNA G-Quadruplex, indicating that the total deformation-polarization energy and desolvation penalty of the ligands are the main terms destabilizing the binding. The pair interaction energy decomposition analysis (PIEDA) between ligand and nucleobases suggest that the main interaction terms are electrostatic and charge-transfer energies supporting the hypothesis that Au(I) ion can be involved in π -cation interactions further stabilizing the ligand-receptor complex. Moreover, the presence of polar groups on the carbene ring, as C=O, can improve the charge-transfer interaction with K^+ ion. These findings can be employed to design new powerful biscarbene-Au(I) DNA-G quadruplex binders as promising anticancer drugs. The procedure described in this work can be applied to investigate any ligand-receptor system and is particularly useful when the binding process is strongly characterized by polarization, charge-transfer and dispersion interactions, properly evaluated by *ab initio* methods.

Introduction

Computational chemistry is a valuable tool in the early stages of drug discovery [1, 2] and several computational approaches can be employed in computer-assisted drug discovery (CADD). Methods based on molecular mechanics (MM) [3] are extensively employed to assess the ligand-receptor binding energy [4-7] but their application might be limited by the force-field (FF) parameterization [8]. When charge-transfer, polarization, and electron transfer phenomena are involved, quantum mechanical (QM) methods [9-12] become necessary, although they can only treat systems with a limited number of atoms. A convenient and mostly used compromise to treat large biological systems is therefore the QM/MM approach [13] where the core of the system is treated by a QM method and the remaining structure by using a MM approach. However, the definition of the QM region and the connection between the MM and QM regions are critical issues.

An alternative powerful QM approach to investigate in detail the ligand-receptor interaction, and in general biological systems, is the *ab initio* fragment molecular orbital (FMO) method [14]. The FMO method allows to split the system into several fragments (e.g., one amino acid per fragment) and the total energy is computed as the sum of the internal energy of each fragment and the interaction energy between each pair of fragments, the so-called pair interaction energy (PIE) (also called “FMO2 approach”) [15]. The total FMO energy can alternatively be computed considering the interaction energy between each set of three (FMO3 [16]) or of four (FMO4 [17]) fragments, leading to an increased accuracy though at a higher computational cost. Therefore, the FMO2 method is the most used FMO approach. In turn, PIE can be analyzed by performing a pair interaction energy decomposition analysis (PIEDA) giving important insights into the chemical nature of the pair interactions [18-20]. Indeed, the FMO method is particularly useful to describe and study the interaction between ligand and receptor (e.g., a protein, DNA) especially when the ligand non-

covalently interacts with the binding site, the most common situation. In this case, the fragment only includes the ligand, and the sum of its PIEs represents the interaction energy between ligand and receptor, E_{LR}^{INT} . Moreover, the analysis of each PIE between the ligand and the binding site residues provides crucial data to boost structure-based drug design.

E_{LR}^{INT} is generally compared with experimental results showing in several cases a satisfactory correlation [21-23]. However, this quantity does not directly represent the ligand-receptor binding energy since it does not take into account the isolated structures of ligand and protein and only provides an approximate description of the ligand-receptor binding strength. A more sophisticated procedure to calculate the real ligand-receptor FMO2 binding energy has been proposed by Fedorov et al. [24]. However, this procedure has seldom been applied as it requires additional FMO calculations of the ligand and receptor isolated structures with a significant increase of the computational effort.

A special class of drugs interacting via non-covalent interactions is that of DNA G-quadruplex (Gq) binders which intercalate into DNA. Gq represents a class of non-canonical secondary structure of DNA, identified in specific DNA guanine rich regions where a cluster of four guanines interact forming a planar cyclic block (G-quartets) [25, 26]. A typical Gq binder is featured by (1) a π -delocalized system; (2) a positive or partial positive charge; (3) positively charged substituents, able to interact with the negatively charged phosphate backbone; and (4) a surface area similar to the guanine tetrads, characterizing DNA Gq [27]. These chemical/structural features can also be found in many metal complexes [28-37] representing an ideal case study to assess the accuracy and the usefulness of FMO2 binding energy. Indeed, in the Gq drug binding process, polarization, charge-transfer and electrostatic interactions can play a crucial role, and all these effects can be properly evaluated by applying an *ab initio* method as FMO [38]. Moreover, this information can be used to improve the design of new and more powerful metal based Gq binders. The discovery of efficient Gq binders may have a great impact in cancer treatment, considering that many studies indicate that drugs able to bind Gq regions can exert anticancer effect [39, R0] as Gq motives were detected in several eukaryotic promoters [41] and oncogenes [42].

A specific class of metal-based drugs, able to interact with DNA Gq, is represented by biscarbene-gold (I) derivatives [43, 44]. As reported by Bertrand et al., $[\text{Au}(9\text{-methylcaffeine-8-ylidene})_2]^+$ and $[\text{Au}(1,3\text{-dimethylbenzimidazol-2-ylidene})_2]^+$, hereafter indicated as **1** and **2** (Fig. 1), respectively, effectively bind DNA Gq, as suggested by FRET-melting assay results [43]. The structural features of the complex formed by **1** and DNA Gq fragment were investigated by resolving the corresponding X-Ray structure (PDB ID: 5CCW), providing structural details about the binding mode of this carbene-gold(I) derivative with DNA Gq fragment [45].

Several computational approaches have been employed so far to study DNA Gq structures and their complexes with several binders, as reviewed by Gil and co-workers [27], nonetheless there are few specific works on the binding of biscarbene-Au(I) ligands to Gq [46, 47].

In the present paper we investigate the binding affinity of **1** and **2** to DNA Gq, by computing the FMO2 binding energy, applying the procedure described by Fedorov et al. [24] with the following two main aims: i) assessing the accuracy and reliability of FMO2 binding energy to describe the ligand-receptor affinity of metal drugs and ii) providing useful new information for designing powerful Au(I)-based Gq binders.

Our results have been compared with theoretical outcomes reported in literature [47] and their consistency is supported by the comparison with experimental data [43].

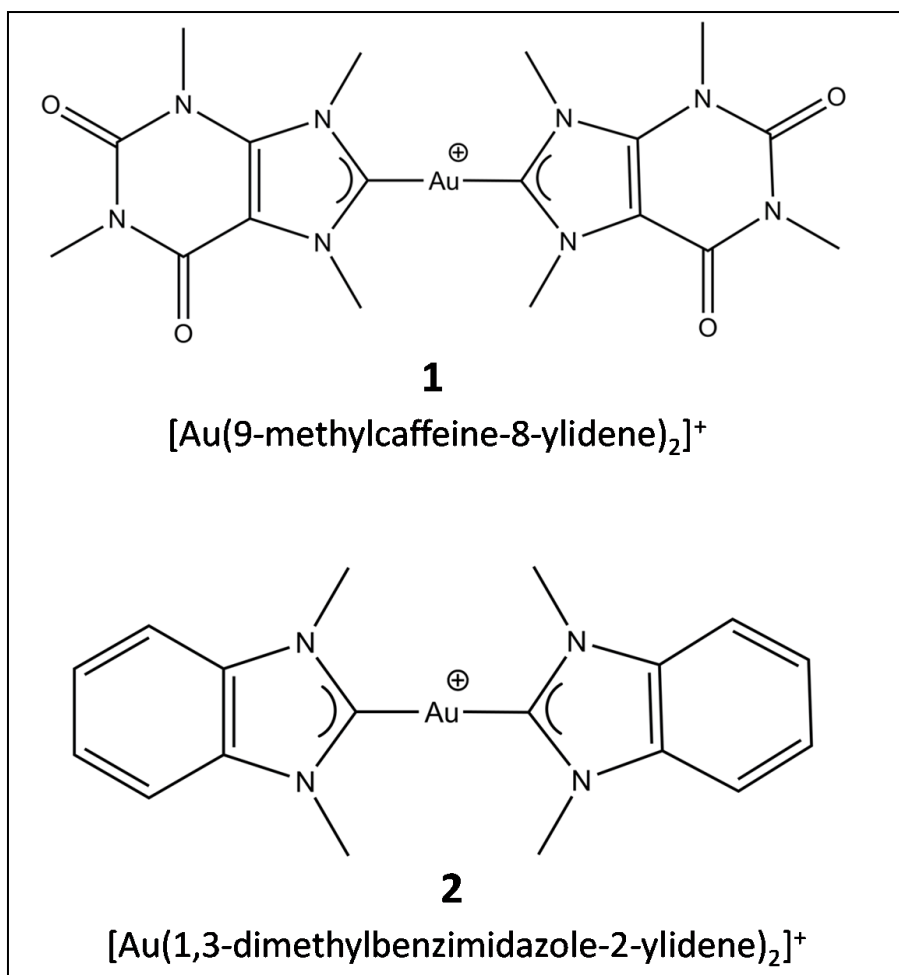


Fig. 1 2D structures of **1**, [Au(9-methylcaffeine-8-ylidene)₂]⁺, and **2**, [Au(1,3-dimethylbenzimidazole-2-ylidene)₂]⁺, investigated in this work

Method

FMO2 binding energy

The *ab initio* FMO approach is a powerful computational method allowing to deal with biological systems, as proteins [48], protein-protein [49, 50] and DNA-protein [51] complexes and ligand-receptor adducts [52], very closely reproducing full *ab initio* properties, as total energies, gradients, dipole moments etc.

The main feature of FMO2 approach consists of the fragmentation of the system in N fragments and the total energy is computed as the sum of internal energies of fragments, E'_i , and fragment pair interaction energies, E_{ij}^{PIE}

$$E = \sum_{i=1}^N E'_i + \sum_{i>j} E_{ij}^{PIE} \quad (1)$$

When the effect of the solvent is computed through the polarization continuum method (PCM) [53], E'_i can be divided into the internal solute energy of the fragment, E''_i , and its solvation energy, E_i^{SOL} , as

$$E'_i = E''_i + E_i^{SOL} \quad (2)$$

E_{ij}^{PIE} is computed as follows from the difference between the internal solute energy of the ij pair and those of the single fragments i and j :

$$E_{ij}^{PIE} = (E''_{ij} - E''_i - E''_j) + E_{ij}^{SOL} + Tr(\Delta D^{ij} V^{ij}) \quad (3)$$

where E_{ij}^{SOL} is the solvation energy of the ij pair with respect to those of the monomers i and j , ΔD^{ij} is the density matrix difference of the dimer ij and the sum of monomers i and j electron densities and V^{ij} is the matrix of the contribution of all other fragments to the electrostatic potential acting upon the dimer ij [24]. PIE can be decomposed in several terms according to pair interaction energy decomposition analysis (PIEDA) [18, 19] as

$$E_{ij}^{PIE} = E_{ij}^{es} + E_{ij}^{ex} + E_{ij}^{ct+mix} + E_{ij}^{disp} + E_{ij}^{sol} \quad (4)$$

where E^{es} , E^{ex} , E^{ct+mix} , E^{disp} and E^{sol} are the electrostatic, exchange repulsion, charge transfer, dispersion, and solvation contributions, respectively. The E^{es} term describes the electrostatic interaction between fragments. E^{ex} is always repulsive and is related to the steric repulsion between close fragments. E^{ct+mix} represents the interaction between the occupied orbitals of a donor and the unoccupied orbitals of the acceptor. E^{disp} is the interaction energy between the instantaneous dipole moments of the two interacting fragments [54]. E^{sol} describes the solvent screening to the pair interaction energies.

If we consider a ligand-receptor complex, LR, where the receptor (R) is either a protein, composed by N fragments (generally taken as the protein residues), or another biological target in which a fragmental structure can be easily envisioned, and L is a small drug molecule (considered as an additional fragment), the total PIE of the ligand is:

$$E_{LR}^{INT} = \sum_{i=1}^N E_{Li}^{PIE} \quad (5)$$

E_{LR}^{INT} is generally used to score the ligand-receptor binding energies and has shown, in several cases, [21-23] a good correlation with the experimental binding data. However, its value does not represent the ligand-receptor binding energy, because it does not include the destabilization polarization and desolvation energies of the fragments in passing from a free to a bound state and is only an estimate of the strength of the ligand-protein interaction, in a specific frozen conformation. It has been shown that E_{LR}^{INT} generally correlates well with experimental data when ligands with similar chemical structures, features, and hitting the same receptor are considered. As mentioned in the Introduction, to properly calculate the ligand-receptor binding energy by using FMO2 method, we must assume the ligand and receptor to initiate the binding process from in their isolated states [24]. Thus, for the formation of the LR complex:

$$L + R \rightarrow LR \quad (6)$$

the FMO2 binding energy, ΔE , can be computed as:

$$\Delta E = E_{LR} - E_R - E_L \quad (7)$$

where E_{LR} , E_R and E_L are the total FMO energies, described by eq. 1, and referred to the optimized structures of the ligand-receptor complex, ligand and receptor, respectively. Thus, according to eq. 2 and 3, ΔE can be rewritten as:

$$\begin{aligned} \Delta E &= \left(\sum_{i=1}^{N+1} E'_i + \sum_{i>j}^{N+1} E_{ij}^{PIE} \right)_{LR} - \left(\sum_{i=1}^N E'_i + \sum_{i>j}^N E_{ij}^{PIE} \right)_R - (E')_L \\ &= \left(\sum_{i=1}^{N+1} E''_i + \sum_{i=1}^{N+1} E_i^{SOL} + \sum_{i>j}^{N+1} E_{ij}^{PIE} \right)_{LR} - \left(\sum_{i=1}^N E''_i + \sum_{i=1}^N E_i^{SOL} + \sum_{i>j}^N E_{ij}^{PIE} \right)_R - (E'' + E^{SOL})_L \end{aligned}$$

$$\begin{aligned} &= \left[\left(\sum_{i=1}^{N+1} E''_i \right)_{RL} - \left(\sum_{i=1}^N E''_i \right)_R - (E'')_L \right] + \left[\left(\sum_{i=1}^{N+1} E_i^{SOL} \right)_{RL} - \left(\sum_{i=1}^N E_i^{SOL} \right)_R - (E^{SOL})_L \right] \\ &\quad + \left[\left(\sum_{i>j}^{N+1} E_{ij}^{PIE} \right)_{LR} - \left(\sum_{i>j}^N E_{ij}^{PIE} \right)_R \right] = \end{aligned}$$

$$= \Delta E' + \Delta E^{PIE} \quad (8)$$

$$= \Delta E'' + \Delta E^{SOL} + \Delta E^{PIE} \quad (9)$$

The FMO2 binding energy is thus the sum of three terms (eq. 9): the first two refer to the variation of the solute internal energy upon binding, $\Delta E''$, which represents the total destabilization polarization energy of the solutes and the desolvation penalty, ΔE^{SOL} , due to the binding process, whereas ΔE^{PIE} represents the differential pair interaction energy, which includes the polarization stabilization due to electrostatic interactions. It is worth noting that $\Delta E''$ implicitly includes the deformation energy, that is the difference in energy between the fragment in the complex and in its isolated state, [24] thus hereafter we refer to $\Delta E''$ as deformation-polarization energy.

Considering eq. 1 and 7, it is possible to rewrite the ΔE^{PIE} term as follows:

$$\Delta E^{PIE} = \left[\left(\sum_{i>j}^{N+1} E_{ij}^{PIE} \right)_{LR} - \left(\sum_{i>j}^N E_{ij}^{PIE} \right)_R \right] =$$

$$\left[\left(\sum_{i>j}^N E_{ij}^{PIE} \right)_{R^*} - \left(\sum_{i>j}^N E_{ij}^{PIE} \right)_R + \left(\sum_{i=1}^N E_{iL}^{PIE} \right)_{LR} \right] =$$

$$= \Delta E_R^{PIE} + E_{LR}^{INT} \quad (10)$$

where R^* and R refer to the receptor in the bound and free state, respectively. ΔE^{PIE} is thus split into two terms describing the variation of the inter-residues interaction energies within the receptor, ΔE_R^{PIE} , passing from the isolated to the bound state, and the PIEs between the ligand and all receptor fragments, i.e., the interaction energy, E_{LR}^{INT} (eq. 5).

Inserting eq. 10 in eq. 9, the FMO2 binding energy can be written as:

$$\Delta E = \Delta E'' + \Delta E^{SOL} + \Delta E_R^{PIE} + E_{LR}^{INT} \quad (11)$$

E_{LR} (eq. 7) can be rewritten separating the energy contributions of all residues (N) of the receptor in the complex (R^*) from the ligand fragment (L^*):

$$E_{LR} = \left(\sum_{i=1}^N E''_i \right)_{R^*} + (E'')_{L^*} + \left(\sum_{i=1}^N E_i^{SOL} \right)_{R^*} + (E^{SOL})_{L^*} + \left(\sum_{i>j}^N E_{ij}^{PIE} \right)_{R^*} + \left(\sum_{i=1}^N E_{iL}^{PIE} \right)_{LR} =$$

$$= \left(\sum_{i=1}^N E''_i \right)_{R^*} + (E'')_{L^*} + \left(\sum_{i=1}^N E_i^{SOL} \right)_{R^*} + (E^{SOL})_{L^*} + \left(\sum_{i>j}^N E_{ij}^{PIE} \right)_{R^*} + E_{LR}^{INT} \quad (12)$$

Substituting equation 12 in eq. 8 and considering eq. 10, the FMO2 binding energy, ΔE , can be finally written as:

$$\Delta E = \Delta E_R'' + \Delta E_L'' + \Delta E_R^{SOL} + \Delta E_L^{SOL} + \Delta E_R^{PIE} + E_{LR}^{INT} \quad (13)$$

Using eq. 13 it is now possible to evaluate the deformation-polarization energy and the desolvation penalty which ligand and receptor undergo to reach the binding pose, as well as the impact of binding on the interaction energies between protein residues. Indeed, the binding with the ligand can modify the conformation and the electrostatic environment of some residues leading to a variation of pair interaction energies (e.g., increasing of H bond distance, breaking of H bonds, steric clashes, polarization, etc.). Thus, the use of ΔE (eq. 13) instead of E_{LR}^{INT} (eq. 5, hereafter simply referred as E^{INT}) leads to a more accurate estimate of the ligand-receptor binding energy.

The magnitude of E_{ij}^{PIE} is related to the number of atoms of the fragment and is therefore size-dependent. A ligand (fragment) with many atoms will have a high E^{INT} . A way to overcome this issue consists of normalizing the interaction energy by the number of heavy atoms (n), obtaining the so-called fragment efficiency, FE [55]:

$$FE = E^{INT}/n \quad (14)$$

The concept of ligand efficiency (LE) is widely used in CADD as a method for comparing molecules according to their average binding energy per atom [56]. It is defined as the measurement of the contribution of each non-hydrogen atom (heavy atom) of the ligand to the binding energy. LE is computed as the ratio of binding free energy (ΔG) and the number of heavy atoms (n) of the ligand [57]

$$LE = \Delta G/n \quad (15)$$

In the same sense, we introduce here the FMO2 ligand efficiency, F2LE, where the FMO2 binding energy, ΔE , computed by including the destabilization polarization and desolvation energies as described in eq. 13, replace ΔG in eq. 15, leading to

$$F2LE = \Delta E/n \quad (16)$$

F2LE therefore represents the average *ab initio* binding energy per atom and can be useful for the comparison of the binding efficiency of a set of ligands.

As a final remark, it is worth noting that ΔE does not include the entropic term and should not be confused with a free binding energy. Some attempts to include entropy in FMO analysis have been described [38, 58, 59].

Computational details

The geometry of DNA G-q (5'-TAGGG(TTAGGG)₃-3') in a complex with three molecules of ligand **1**, **Gq-1₃**, was retrieved from the protein data bank (PDB ID: 5CCW) [45]. The DNA structure was refined by using the protein preparation tool [60, 61] and Macromodel [61] to fix H atoms and atom charges. The terminal RPO₃ group (5' position) of the sugar-phosphate backbone, present in the original 5CCW structure, has been treated as RPO₄²⁻.

The geometries of biscarbene-Au(I) ligands, **1** and **2**, were optimized at B3LYP/6-311+G** level of theory, adopting the LANL2DZ pseudopotential for Au atoms, by using Gaussian suite [62].

Each ligand molecule reported in the X-Ray structure binds the receptor at three different binding sites, I-III; as shown in Fig. 2A, which are basically represented by the following guanine nucleotide (DG) pairs: DG11•DG5, DG15•DG21 and DG9•DG3, respectively (Fig. 2B).

The binding efficiency of **1** for each binding site was evaluated separately so to obtain three LR complexes, each with one **1** molecule maintained at a different binding site: Gq-1(I), Gq-1(II) and Gq-1(III) complexes. Starting from these complexes we built the corresponding ones for ligand **2** (Gq-2(I), Gq-2(II) and Gq-2(III)) by manually superimposing structure of **2** with **1**.

The free DNA Gq structure and the seven LR complexes, such as Gq-1₃, Gq-1(I), Gq-1(II), Gq-1(III), Gq-2(I), Gq-2(II) and Gq-2(III), were minimized using density functional tight-binding (DFTB) theory as implemented in xTB software [63, 64], adopting the GFN2-xTB method [65]. The effect of water solvation was simulated by employing the GB/SA method implemented in the xTB software.

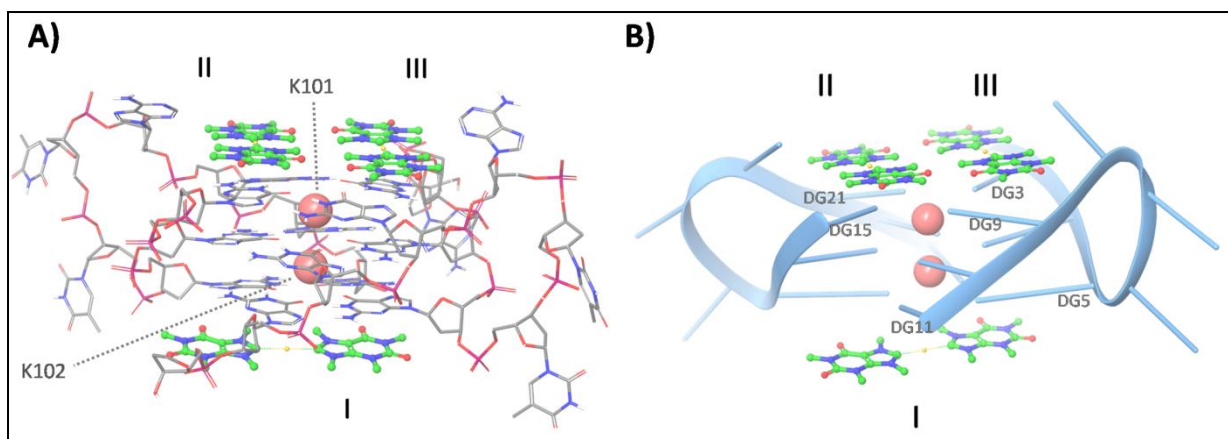


Fig. 2 a) Optimized X-Ray structure of Gq with three ligand **1** molecules placed at the three binding poses (I, II and III). The K⁺ ions are represented by pink spheres, and ligand **1** molecules are shown in green ball and stick style. b) Gq-1 complex where DNA is represented by using blue cartoon style. The nucleotides (DG) interacting directly with the ligand molecules are shown in gray

Then, the optimized geometries of Gq-ligand complexes and of the isolated species were used as input for FMO2 single point calculations at RI-MP2/6-31G* level of theory [66-69], and PIEDA was also performed.

The water solvation effect was simulated by the PCM[1] method, by computing the repulsion and dispersion contributions by the empirical method of Floris and Tomasi [70], using a high density of tesseræ on the cavity surface (NTSALL=240) and FIXPVA as tessellation scheme [71]. The solvent screening effect was simulated adopting the *local* solvent screening model. The cavities holding the solute were generated by adopting the simplified united atomic radii (radii=suahf). Charge compensation was included (ICOMP=2) and cavitation energy was computed by Claverie-Pierotti method (ICAV=1) at 298 K [72, 73].

To overcome the charge instability that might occur during SCF calculations with metal atoms, the energy error threshold for Pulay's DIIS interpolation was set to 2.0 hartree (ETHRSH=2.0) and the density matrix convergence at which to switch from DIIS to second order SCF orbital optimization (SOSCF) was set to 0.005 (SWDIIS=0.005). The Au atom was treated by adopting the triple zeta model core potential (MCP-TZP) [74]. All FMO calculations were performed by using GAMESS-US package [75].

The DNA Gq structure was systematically fragmented at N-glycosidic bond, N1-C1', and at O-C5' bond, to separate the nucleobase (guanine, G) and 2'-deoxyribose sugar and a phosphate group into distinct fragments, as reported in Fig. 3 [76]. G10, G22 and the K⁺ ion (atom ID in 5CCW pdb file: K102) were considered as a unique fragment as well as G16, G4 and the other K⁺ atom (K101), as shown in Fig. S1.

The FMO results were analyzed and elaborated to compute the FMO2 binding energies, ΔE , FE, F2LE and all energy terms described in eq. 8, 9, 11 and 13 for each investigated complex.

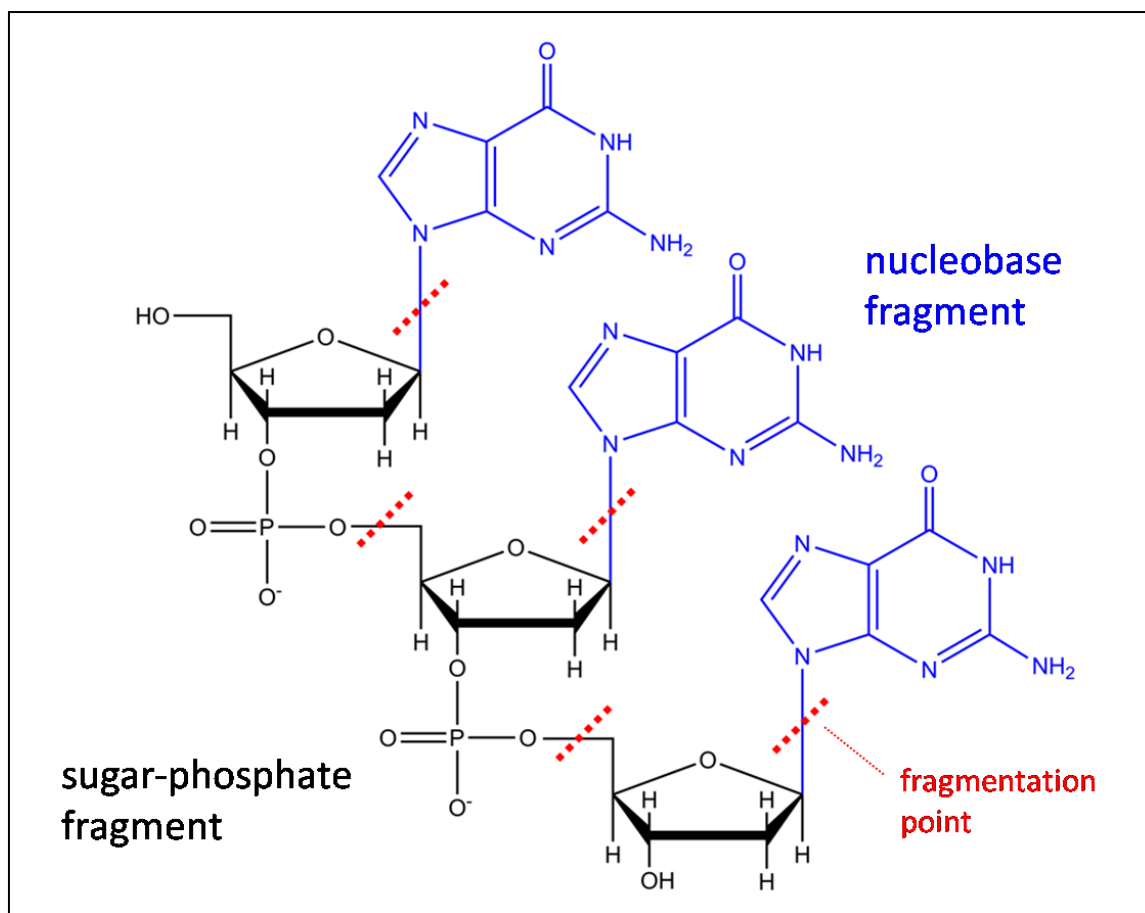


Fig. 3 Fragmentation strategy used in this work. Two types of fragments are obtained: sugar-phosphate (black) and nucleobase (blue) fragments. The fragmentation point is represented by a red dashed line

Results

The structures of Gq-1₃, Gq-1(I), Gq-1(II), Gq-1(III), Gq-2(I), Gq-2(II) and Gq-2(III) optimized at DFTB level are shown in Fig. 2, S2, S5 and S7. The binding poses of **1** in position I-III are superimposable to the X-Ray structure, suggesting that negligible geometrical adjustments occurred during geometry optimization. Comparing the binding poses of **1** and **2** in binding site I (Fig. S3 and S4), we found that **1** is not perfectly parallel to the G5•G11 plane but is rotated around the C-Au-C axis with two C=O and two N-CH₃ groups heading toward K⁺(102) while **2** is rotated toward the opposite direction leading to an increase and a reduction of K⁺(102)⋯(N)CH₃ and (N)CH₃⋯G5•G11 distances, respectively, as shown in Fig. S4. On the contrary, the binding poses of **1** and **2**, in sites II (Fig. S6) and III (Fig. S8) are rather similar.

FMO2 binding energies, ΔE , were computed according to eq. 7 for the Gq-1(I), Gq-1(II) and Gq-1(III) complexes and are reported, together with the corresponding energy decomposition components, in Table 1.

ΔE values are negative for each investigated complex indicating that the formation of the Gq-ligand complex is a favored process. For both ligands the most significant interactions take place at position I, with ΔE of -320.8 for **1** and -176.6 kcal/mol for **2**. Considering the binding sites II and III, the ΔE values computed for **2** are more negative than the corresponding ones for **1**, suggesting a greater

affinity for these sites. However, considering ΔE values averaged over position I, II and III (-171.5 kcal/mol for **1** and -146.5 for **2**), **1** can bind DNA Gq more effectively than **2**. As reported above, ΔE can be divided in two terms, $\Delta E'$ and ΔE^{PIE} , which describe the variations of the fragment internal energies and that of the PIEs, respectively, passing from L and R to LR complex. As shown in Table 1, $\Delta E'$ is positive for all LR complexes, and significantly larger for **1**. Moreover, for both ligands, the $\Delta E'$ for position I is larger than for II and III. Thus, $\Delta E'$ is always unfavorable and highlights how the LR binding process implies a destabilization due to deformation and polarization effects in solution. ΔE^{PIE} values, representing the driving force of the binding process, are instead always attractive. Interestingly, while for ligand **2** ΔE^{PIE} has comparable values for all three complexes, with only a slightly more negative value for Gq-2(I), for ligand **1** ΔE^{PIE} (Gq-1(I)) is more than twice negative compared to Gq-1(II) and Gq-1(III).

Table 1 FMO2 binding energies values, ΔE , and its components, $\Delta E'$ and ΔE^{PIE} (eq. 8), representing the variations of the fragment internal energy and of pair interaction energy (PIE), respectively. All values are reported in kcal/mol

Complex	ΔE	$\Delta E = \Delta E' + \Delta E^{PIE}$	
		$\Delta E'$	ΔE^{PIE}
Gq-1(I)	-320.8	+139.9	-460.7
Gq-1(II)	-86.0	+119.2	-205.2
Gq-1(III)	-107.7	+95.2	-202.9
<i>average</i>	<i>-171.5</i>	<i>+118.1</i>	<i>-289.6</i>
Gq-2 (I)	-176.6	+71.0	-247.6
Gq-2(II)	-123.5	+52.7	-176.2
Gq-2(III)	-139.4	+38.8	-178.2
<i>average</i>	<i>-146.5</i>	<i>+54.2</i>	<i>-200.7</i>

According to eq. 11, ΔE can be written considering that $\Delta E'$ and ΔE^{PIE} correspond to $\Delta E'' + \Delta E^{SOL}$ and $\Delta E_R^{PIE} + E^{INT}$, respectively. The analysis of these terms can reveal precious information about the binding process between Gq and carbene-Au(I) ligands. Interestingly, ΔE^{SOL} is always positive for both Gq-**1** and Gq-**2** complexes, with the largest values computed for Gq-1 adducts, indicating a significant desolvation penalty passing from the isolated to the bound state. The internal solute energy, $\Delta E''$, is positive for ligand **1**, for all binding sites, and for Gq-2(I) complex, reflecting the destabilization due to deformation and polarization effects of receptor and ligand upon binding. On the contrary, slightly negative values of $\Delta E''$ were obtained for Gq-2(II) and Gq-2(III), indicating that the fragment conformations in the bound states are more stable than the isolated ones. This trend was not found for Gq-1 complexes.

ΔE_R^{PIE} is positive for all binding sites – and quite large but for Gq-1(I) – indicating that the formation of the LR complex reduces the attractive contacts between DNA fragments. E^{INT} terms are instead always attractive, especially for Gq-1(I). Hence, the presence of the ligand apparently reduces the interaction among DNA fragments, but the much larger negative values of E^{INT} compensate the unfavorable ΔE_R^{PIE} and $\Delta E'$, leading to the formation of stable Gq-ligand complex.

Table 2 Decomposition of $\Delta E'$ and ΔE^{PIE} terms, as described by eq. 11, for Gq-1 and Gq-2 complexes, considering the I, II and III binding sites. All energy values are reported in kcal/mol

Complex	$\Delta E'$	$\Delta E' = \Delta E'' + \Delta E^{SOL}$		ΔE^{PIE}	$\Delta E^{PIE} = \Delta E_R^{PIE} + E^{INT}$	
		$\Delta E''$	ΔE^{SOL}		ΔE_R^{PIE}	E^{INT}
Gq-1(I)	+139.9	+71.1	+68.8	-460.7	+87.9	-548.6
Gq-1(II)	+119.2	+29.5	+89.7	-205.2	+219.9	-425.1
Gq-1(III)	+95.2	+23.7	+71.4	-202.9	+208.0	-410.9
Gq-2(I)	+71.0	+26.2	+44.7	-247.6	+149.8	-397.4
Gq-2(II)	+52.7	-4.0	+56.7	-176.2	+176.1	-352.3
Gq-2(III)	+38.8	-9.3	+48.1	-178.2	+169.3	-347.5

To understand the nature of the deformation-polarization energy and desolvation penalty, we have further decomposed $\Delta E''$ and ΔE^{SOL} into the contributions of DNA Gq (receptor) and of the ligand (eq. 13), as reported in Table 3. The first term, $\Delta E_R''$, is positive when the binding occurs at site I, with 28.3 kcal/mol for Gq-1(I) and only 0.7 kcal/mol for Gq-2(I). When the ligands bind to site II and III $\Delta E_R''$ is negative, with slightly lower Gq-2 complexes values. On the contrary, the total deformation and polarization energy of the ligands, $\Delta E_L''$, is always positive, leading to a significant destabilization, with higher values computed for ligand **1**. Moreover, $\Delta E_L''$ is larger for the binding site I, for both **1** and **2**.

This suggests that the largest contribution to the solute deformation and polarization destabilization energy can be almost entirely attributed to the ligand, representing the energetic tribute that must be paid to adopt the binding pose. The two carbene rings in **1** and **2** free structures are indeed perpendicular (Fig. S9), whereas they become coplanar upon binding which likely involves a conformational penalty. On the other hand, DNA fragments undergo a structural stabilization in the binding process to sites II and III and a negligible/small destabilization upon binding to site I.

ΔE_R^{SOL} is characterized by low positive values with the exception of Gq-1(II), where it has a significantly larger value of +24.7 kcal/mol, and of Gq-2(I), where it is slightly negative. ΔE_R^{SOL} values are close to zero for Gq-1(I) and Gq-2(III), suggesting that the interaction between Gq and the solvent does not significantly change from the free to the bound state. The small negative value for Gq-2(I), -6.9 kcal/mol, indicates that the solvation energy of this DNA region is enhanced by the ligand binding. On the other hand, ΔE_L^{SOL} is always positive with average values of 65.5 and 49.1 kcal/mol for **1** and **2**, respectively. As expected, the ΔE_L^{SOL} at the three different binding sites shows similar values, within the range 63.3 – 68.2 kcal/mol for **1**, and in the range 47.8 – 51.6 kcal/mol for **2**.

Similarly, to what observed for $\Delta E''$, ΔE^{SOL} represents the main term that contributes to the total desolvation penalty indicating that, passing from the free to the bound state, the ligand desolvation energy is significantly higher compared to that of Gq. It is worth noting that ΔE_L^{SOL} calculated for **1** is higher than for **2**, as expected because of its higher polarity given by the nitrogen and oxygen atoms on the outer six-member ring.

Table 3 Decomposition of total deformation-polarization energy, $\Delta E''$, and total desolvation energy, ΔE^{SOL} , into ligand (**1** and **2**) and receptor (Gq) contributions. All values are reported in kcal/mol

Complex	$\Delta E''$	$\Delta E'' = \Delta E_R'' + \Delta E_L''$		ΔE^{SOL}	$\Delta E^{SOL} = \Delta E_R^{SOL} + \Delta E_L^{SOL}$	
		$\Delta E_R''$	$\Delta E_L''$		ΔE_R^{SOL}	ΔE_L^{SOL}
Gq-1(I)	+71.1	+28.3	+42.8	+68.8	+0.6	+68.2
Gq-1(II)	+29.5	-7.2	+36.7	+89.7	+24.7	+64.9
G-1(III)	+23.7	-8.6	+32.3	+71.4	+8.2	+63.3
Gq-2(I)	+26.2	+0.7	+25.5	+44.7	-6.9	+51.6
Gq-2(II)	-4.0	-11.4	+7.4	+56.7	+8.7	+48.0
Gq-2(III)	-9.3	-15.4	+6.1	+48.1	+0.3	+47.8

While ΔE provides exhaustive information on binding process, taking into account the ligand and receptor in the free as well as in the bound state, E^{INT} gives a measure of the interaction strength between the ligand and all receptor fragments, nucleobase and sugar-phosphate fragments in this case. Fig. 4 summarizes the total PIEDA of the examined complexes **1** and **2**, by reporting the contribution of each energy term in eq. 4. The most important attractive term for both **1** and **2**, E^{es} , is related to electrostatic interactions, with average values of -610.7 and -609.6 kcal/mol; these close values suggest that the functionalization of the caffeine ring does not significantly affect the total inter-fragment electrostatic interactions. E^{disp} and E^{ct+mix} terms are also attractive, with comparable values for **1** and **2** when the same binding pose is concerned. In general, calculations show that all the attractive terms - E^{es} , E^{disp} , E^{ct+mix} - have the lowest value for position I, suggesting that the strongest interactions ligand-DNA Gq structure occur at this site.

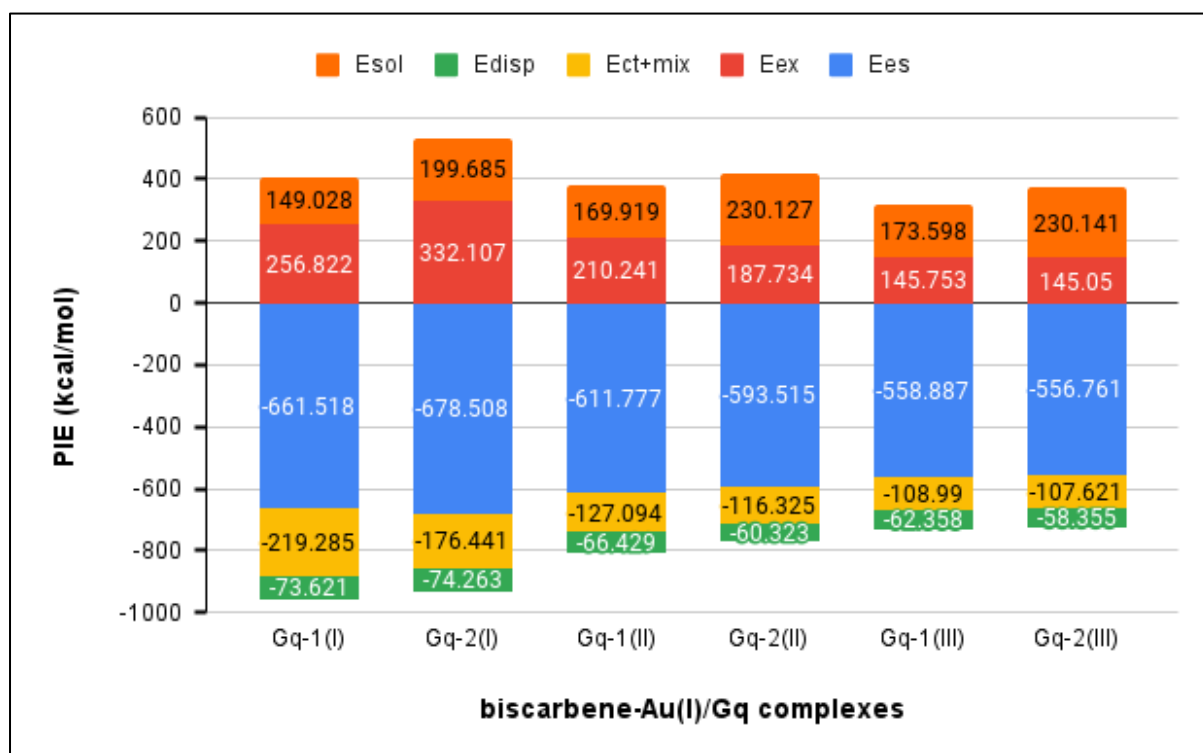


Fig. 4 Bar diagram of total PIEDA for Gq-1 and Gq-2 complexes, considering the three different binding regions I, II and III. E^{es} , E^{ex} , E^{ct+mix} , E^{disp} and E^{sol} are the electrostatic, exchange repulsion, charge transfer, dispersion and solvation energies, respectively

E^{ex} , accounting for the steric interaction between ligand and receptor, is always repulsive. This term represents the most important contribution to the repulsive energy for both ligands. As shown in Fig. 4 (6), while comparable E^{ex} values were computed for positions II and III, a large difference was found for **1** and **2** at position I. A detailed analysis of E_{Li}^{PIE} indicates that the relevant E^{ex} term (101.3 kcal/mol) computed for **2**(I) is mainly due to 2-G11 interaction, as shown in Table S2. This large value can be ascribed to the specific binding mode of **2**(I), where the rotation on C-Au-C axis leads to a reduction of (N)CH₃...G5•G11 distances increasing the steric clashes (Fig. S4).

E_{sol} is also repulsive and is larger in the adduct formed by **2**. Notably, in this case E^{sol} is referred to solvation energy of the pair formed by the ligand and the DNA fragment.

Fig. 5 reports the contribution of each E_{Li}^{PIE} term to total PIE, E^{INT} , of ligand **1** with DNA-Gq for all three positions I-III, see eq. 5. The most negative E^{INT} value was found for position I (Table 2). The most attractive interaction occurs with fragment 7 which includes the ion K⁺ (102) and two nucleobases (G10 and G22). As reported in Table S2 and schematized in Fig. S10-S12, the PIEDA indicates that this interaction is mainly due to electrostatic (-133.2 kcal/mol) and charge-transfer energy (-167.5 kcal/mol). These two energy contributions play a crucial role in the interactions with G10•G22•K102 fragment. Analogously, when positions II and III are considered, the most attractive interaction of **1** is found with fragment 19, which includes G16•G4•K101, although less attractive than 1(I)-fragment 7, mainly coming from the electrostatic and charge-transfer contributions. A somehow similar PIEs trend was observed for ligand **2** in position I-III as shown in Fig. 6, S10-S12 and Table S2. These features indicate that both ligands in binding pose I can establish stronger electrostatic and charge-transfer interactions than in position II and III, thus leading to higher overall binding energies.

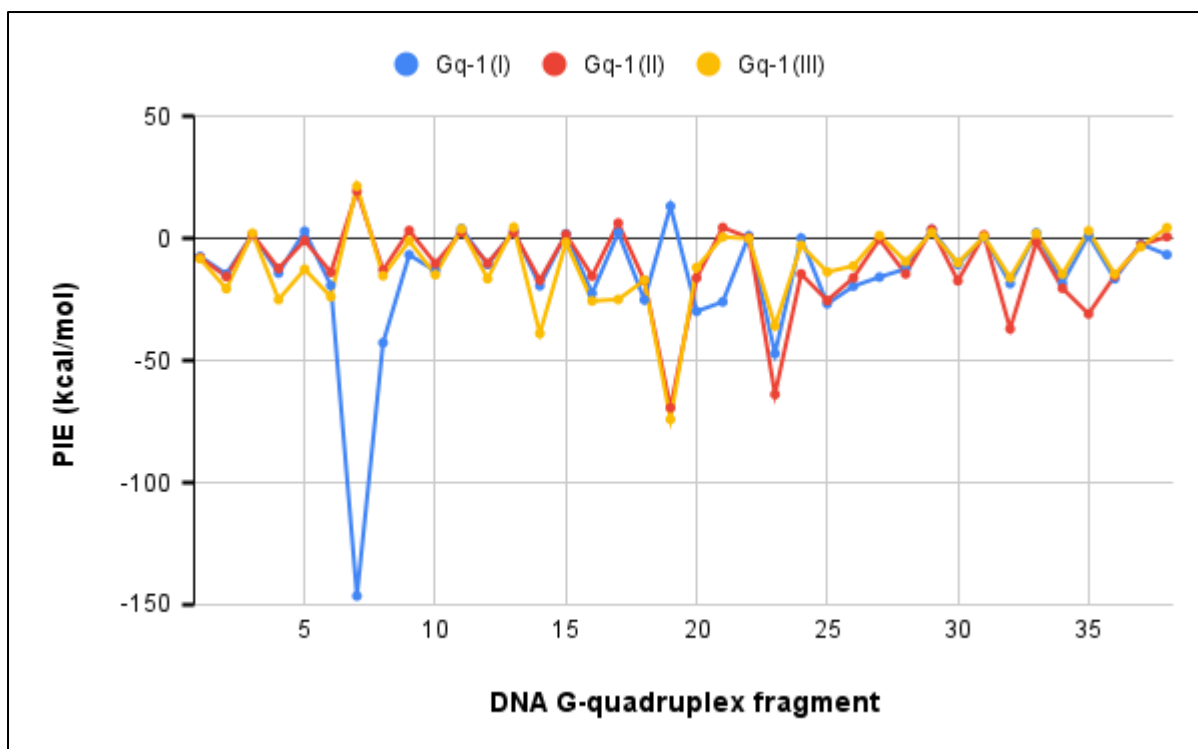


Fig. 5 E_{Li}^{PIE} values for the interaction between Gq fragments and ligand 1 in the binding sites I, II and III, reported by using blue, red, and yellow lines, respectively

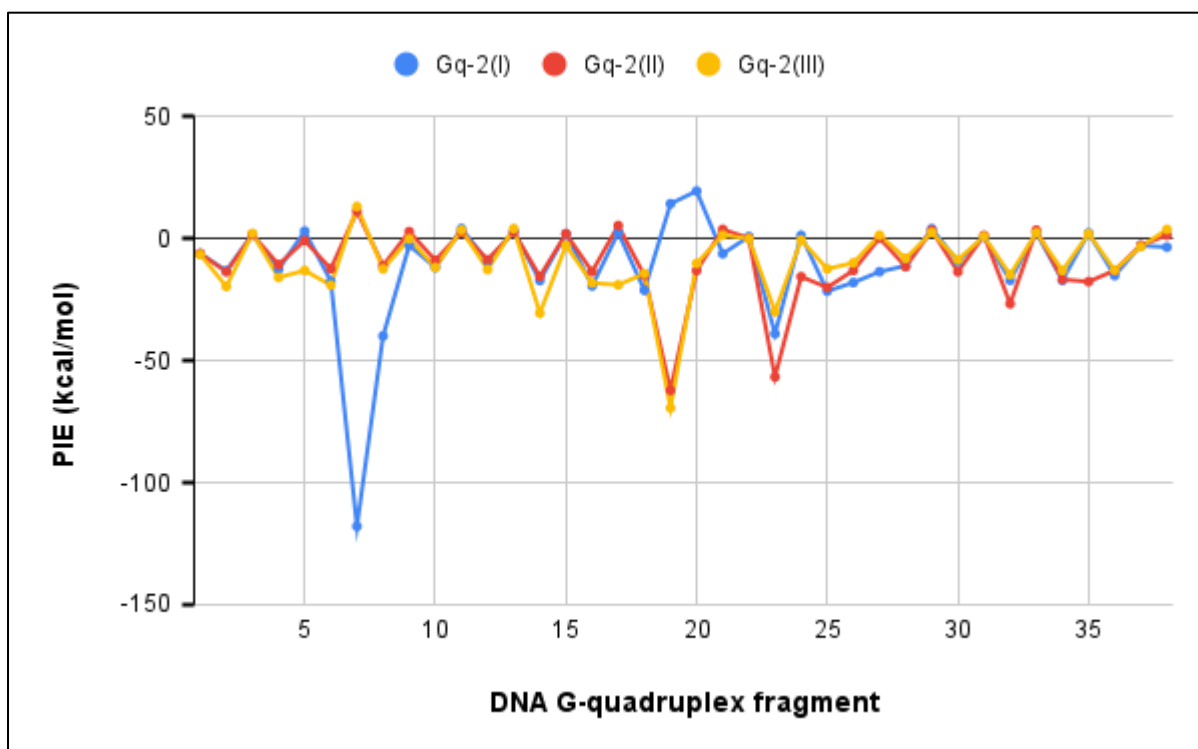


Fig. 6 E_{Li}^{PIE} values for the interaction between Gq fragments and ligand 2 in the binding sites I, II and III, reported by using blue, red, and yellow lines, respectively

Indeed, as shown in Fig. 7, ligand **1** is characterized by several chemical modifications with respect to **2** that significantly change the molecular electrostatic potential (MEP) localizing the negative charged regions especially on the oxygen end of the C=O moieties and two of them are oriented toward the K⁺ ion.

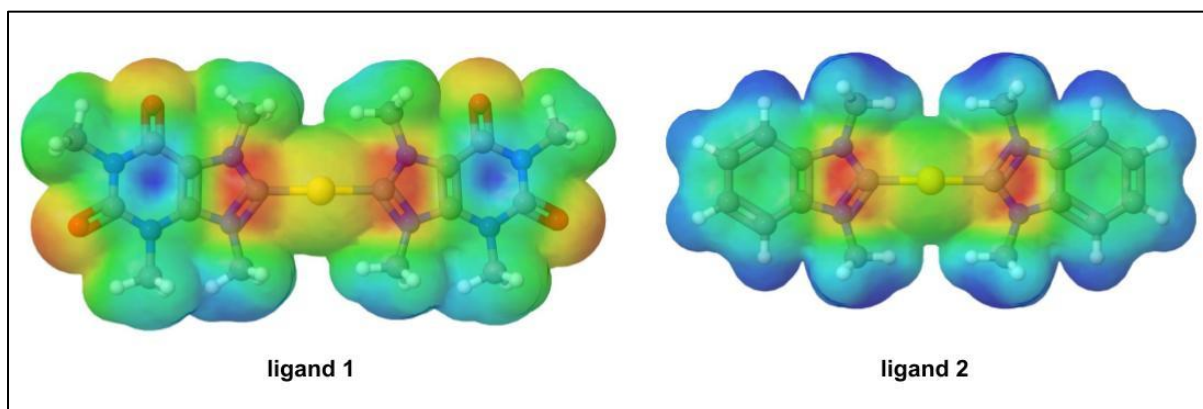


Fig. 7 molecular electrostatic potential of ligand **1** (left) and **2** (right) computed for the isolated molecules in their binding conformations. Different colors indicate different electronegative regions: red and blue are the most negative and positive regions, respectively, while orange, yellow, green and light blue are in between

As a result, **1** adopts a specific binding orientation at position I with one O atom of the C=O groups very close (5.7 Å) to K⁺(102) ion, improving the electrostatic and charge-transfer interactions (Figs. S3 and S4). Moreover, for both **1**(I) and **2**(I), one CH₃ is placed exactly on the top of K⁺(102), along the K⁺(102)-K⁺(101) axis, with an angle close to 180°. This arrangement should lead to an electrostatic repulsion with **2**, considering that CH₃ groups are also positively charged, which induces a rotation around C-Au-C and explaining the different binding pose with respect to **1** (Fig. S4). The analysis of the PIE attractive terms (E^{es} , E^{disp} and E^{ct+mix}) between ligands and the pair of underlying nucleobases reflects the asymmetric binding mode mainly due to Au⁺- π (guanine) electrostatic and charge transfer and to π (benzimidazole)- π (guanine) interactions. For instance, for Gq-1(I), the PIEs for **1**(I)-G5 and **1**(I)-G11 are -6.6 and -25.8 kcal/mol, respectively. This can be explained by observing that one caffeine moiety lies almost exactly above G5 (Fig. S3A) maximizing the π - π interactions, while the other carbene ring only partially superimposes over G11 but lies below the Au(I) ion maximizing the Au⁺- π (C=O of guanine) electrostatic and charge transfer interactions. Correspondingly, the most important contributions to the PIE between **1** and the pair of underlying G5 and G11 nucleobases are E^{es} , E^{disp} and E^{ct+mix} . E^{disp} is negative corresponding to attractive π - π interactions, with a higher value for G5 than for G11 (-19.4 vs. -16.6 kcal/mol) reflecting a better π - π superposition. A negative E^{es} value is instead observed only for G11 (-16.6 Kcal/mol) due to the interaction with Au(I) ion, and a repulsive electrostatic interaction is observed for G5 (E^{es} 15.2 kcal/mol). A similar trend in E^{es} , E^{disp} and E^{ct+mix} is observed for the ligand-nucleobase interactions in the II (G15•G21) and III (G9•G3) binding sites.

PIE graphs (Figs. 5 and 6) are generally characterized by scattered profiles, with very small positive values computed for nucleobase fragments, exception for those nucleobase pairs directly interacting with ligands. Attractive interactions are instead obtained for the two G16•G4•K101 and G10•G22•K102 fragments, which include a K⁺ ion, and for the sugar-phosphate fragments which are negatively charged.

E^{INT} was also computed for the Gq-1₃ complex, where all three positions are occupied by a **1** molecule and results are shown in Table S1. For sites II and III E^{INT} is slightly lower (20-40 kcal/mol) and for site I is slightly higher (25 kcal/mol) than for the monoadducts, and the PIEDA results show that the magnitude of each energy contribution is also almost unchanged. Interestingly, the PIE between the three ligands is repulsive with 30.1, 23.1 and 24.2 kcal/mol for 1(II)-1(III), 1(I)-1(II), 1(I)-1(III), respectively.

F2LE values computed for **1** and **2**, at the three binding sites, are reported in Table 3. It is worth noting that ligands **1** and **2** include 31 and 23 heavy atoms, respectively, and the F2LEs are therefore closer than the corresponding ΔE values. Indeed, the F2LE for Gq-1(I) and Gq-2(I) are -10.3 and -7.7 kcal/mol, respectively, suggesting a lower difference in the binding efficiency of the two ligands than that obtained according to the ΔE values. Moreover, the F2LE values for positions II and III are more favorable for ligand **2** than for **1**.

As E^{INT} is also size dependent, FE values were computed according to eq. 14 (Table 4). The FEs for the position Gq-1(I) and Gq-2(I) are -17.7 and -17.3 kcal/mol, respectively, suggesting very similar interaction energies per atom. Hence, on the basis of FE results, the two ligands should have the same ligand efficiency for the receptor, whereas ΔE values indicate **1** to bind significantly stronger than **2**. However, FE values do not include the destabilization due to deformation and polarization energy and to desolvation penalty, which significantly affect the binding energy of the two ligands as previously discussed.

Table 4 FMO2 ligand efficiency, F2LE, fragment ligand efficiency, FE, and FMO binding energy computed after removing K⁺ ions from the input structures, $\Delta E^{(no\ K^+)}$, for ligand **1** and **2** in the I, II and III binding poses. All values are reported in kcal/mol

Complex	ΔE	F2LE ^a	FE ^a	$\Delta E^{(no\ K^+)}$
Gq-1(I)	-320.8	-10.3	-17.7	-12.3
Gq-1(II)	-86.0	-2.8	-13.7	28.3
Gq-1(III)	-107.7	-3.5	-13.3	10.6
Gq-2(I)	-176.6	-7.7	-17.3	33.8
Gq-2(II)	-123.5	-5.4	-15.3	-10.2
Gq-2(III)	-139.4	-6.1	-15.1	-17.2

^a Heavy atoms per ligand: 31 and 23 for **1** and **2**, respectively.

The computed ΔE terms are large negative values compared to typical binding energies and, as described above, for each binding site the most attractive E^{INT} pair interaction is found for the fragment containing the K⁺ ion nearest to the ligand. This suggests that K⁺ ions may play a role in determining large attractive ΔE values. We therefore performed additional calculations after removing the K⁺ ions from the input structures and the resulting binding energy values, $\Delta E^{(no\ K^+)}$, are reported in Table 4.

Interestingly, all the $\Delta E^{(no\ K^+)}$ values show a magnitude comparable with typical binding energy values although negative binding energies were only found for Gq-1(I) (-12.3 kcal/mol), Gq-2(II) (-10.2 kcal/mol) and Gq-2(III) (-17.2 kcal/mol).

An extensive analysis of the energy terms of fragment 7 (G10•G22•K102) and 19 (G16•G4•K101) reveals that $\Delta E_{(frag\ 7)}^{PIE}$ and $\Delta E_{(frag\ 19)}^{PIE}$ show very attractive values when K^+ ions are included in the input structures (Table S3). In such cases a large negative value of the $\Delta D^{ij*}V^{ij}$ term (eq. 3) is found for their pair interactions in the bound state, that is the explicit embedded charge transfer energy. On the contrary, the corresponding $\Delta E^{PIE(no\ K^+)}$ are very small indicating that PIEs of fragment 7 and 19 are not significantly affected by the presence of the ligand.

This results suggests that the presence of K^+ ions determines an increase of the charge transfer energy when K^+ containing residues are involved, which is overestimated in the presence of ligands, producing large ΔE values.

A reduced solvent screening effect, ascribable to the adopted local model, might also contribute to large ΔE values. To address this question, we performed a set of calculations for ligand **1**, Gq, 1-Gq(I), 1-Gq(II) and 1-Gq(III) by using the partial screening method, able to more accurately describe the solvent screening effect between opposite charged ligand and receptor [77]. Here we used the area scaling tessellation method (GEPOL-AS) including the dispersion and repulsion corrections. The energy values computed with partial solvent screening are hereafter indicated as \mathcal{E} (e.g., \mathcal{E}^{INT} , $\Delta\mathcal{E}$, etc.).

As shown in Table S4, the calculated $\Delta\mathcal{E}$ are very close to the corresponding ΔE values (computed with local solvent screening), with \mathcal{E}^{INT} smaller than E^{INT} due to the significant improving of the solvent screening effect, as expected (Figs. S13-S16).

$\Delta\mathcal{E}$ values therefore reproduce the binding affinity trend found for ΔE (I>III>II). Notably, the most negative term of \mathcal{E}^{INT} corresponds to the PIE of the dimer formed by the ligand and the nearest fragment containing K^+ ion (e.g., 1(I) and fragment 7) and has almost the same value independent on the solvent screening model used in the calculations (Figs. 13-16). The energy terms analysis of fragments 7 and 19 once more shows large attractive $\Delta\mathcal{E}_{(frag\ 7+19)}^{PIE}$ values due to large $\Delta D^{ij*}V^{ij}$ terms computed in the presence of ligands (Table S5). This result confirms that the embedded charge transfer energy overestimation for pair interactions involving the K^+ containing fragments is the main cause determining large ΔE values.

However, it is worth noting that the magnitude of ΔE values computed in this work for biscarbene-Au(I)-Gq complexes is consistent with FMO2 binding energy results obtained by Prato et al. for substituted naphthalene diimide Gq binders which demonstrated a significant correlation with experimental melting temperatures ($R^2=0.9719$) [38]. This suggests that the ΔE values, though quantitatively too large, can be properly used to determine the relative binding strength of similar ligands hitting the same Gq structures.

Discussion

Metal based drugs have shown promising chemical features to represent potential DNA Gq binders exerting antitumor effect [27, 28]. This evidence expands the possible mechanisms of action of metal drugs, which are generally assimilated to the covalent binding of the metal atom to biological targets, as for instance to DNA guanine (N7 atom) or to protein specific amino acid side chains (e.g., cysteine and methionine). Computational chemistry can offer a valuable support and improvement to the design of more powerful and selective metal based Gq binders. With this aim, we applied the *ab initio* FMO method to investigate the binding affinity of two biscarben-Au(I) derivatives, **1** and **2** (Fig. 1), that demonstrated to effectively bind DNA Gq.

In the X-Ray structure (PDB ID: 5CCW), ligand **1** is located at three different binding sites (I-III): we separately evaluated ΔE for **1** and **2** ligands at each position. Both ligands show the most negative ΔE

values when bound at position I suggesting that this could be the site with most affinity. ΔE computed for Gq-1(I) and Gq-2(I) are -320.8 and -176.6 kcal/mol, respectively, indicating that both ligands are characterized by high binding strengths, with ligand **1** showing much higher affinity. This can be ascribed to the specific binding pose computed for Gq-1(I) where the ligand can adopt an optimal position to maximize the interaction with the nearest $K^+(102)$ ion, in addition to π - π and Au^+ - π interactions with the underlying nucleobases. In particular, ligand **1** is characterized by four carbonyl groups that determine a local negative MEP and two of them are oriented toward the $K^+(102)$ ion improving the electrostatic and charge-transfer interactions.

This evidence agrees with experimental data obtained by FRET-melting assays [43] which showed a greater propensity of Gq for ligand **1** with respect to **2**, when a concentration of 50 μ M of unlabeled duplex DNA competitor ds17 was used. Indeed, although the two binders show comparable affinity with a ds17 concentration of 15 μ M, only ligand **1** exceeded the selectivity threshold in presence of an excess of ds17 (50 μ M) [43].

The main structural differences between **1** and **2** are i) the presence of two additional C=O moieties and the presence of two nitrogen atoms fused in the phenyl ring of ligand **1** and iii) two CH_3 groups on the phenyl ring of **1** (Fig. 1). Since E^{INT} is size dependent, as discussed above, it can assume a more negative value for ligands with a larger number of atoms and it is thus expected that the 9-methylcaffein-8-ylidene compared to the 1,3-dimethylbenzimidazole-2-ylidene scaffold may form more interactions with DNA. On the other hand, as shown in Table 3, FE values and E^{INT} for Gq-1(I) and Gq-2(I) are very similar (-17.7 and -17.3 kcal/mol, respectively), indicating that each non-hydrogen atom of **1** and **2** experiences almost the same average per atom interaction energy.

With the same approach, we computed the F2LE to account for the impact of the ligand size on ΔE (Table 4), and obtained -10.3 and -7.7 kcal/mol for Gq-1(I) and Gq-2(I), respectively. Indeed, in our opinion, the binding affinities trend resulting from FRET-melting assays [43] is even better reproduced by using F2LE in place of ΔE or FE values, thus, suggesting that the former energy term can be a promising parameter to compare the binding strength of these ligands. Moreover, F2LE might be improved including other properties such as lipophilicity, combinations of physicochemical properties, functional group and entropy contributions as already done for classic LE [56].

The ΔE value provides an effective binding energy estimation since it considers the structure of the receptor and ligands in the isolated states (eq. 13). Our results indicate that the main terms opposing to binding are the desolvation penalty and the ligands deformation-polarization energy which are larger for **1** than for **2**: **1** pays a higher energy cost to assume the binding pose to occupy a specific receptor site. Ligand **2**, probably due to its higher lipophilicity, is characterized by a lower solvation penalty.

Moreover, **1**, characterized by a larger polarity (Fig. 7), establishes strongest interactions with G-q, especially at site I, as indicated by E^{INT} values and PIEDA. Thus, our results suggest that to design a powerful metal based Gq binders one needs to take into account the molecular polarity and the hydrophilicity/lipophilicity balance of the planar ligands coordinated to the metal atom. In fact, a large number of polar moieties can increase the interaction with Gq, but might lead to a significant solvation penalty.

A potential issue in the use of FMO2 binding energy values may be represented by the lack of entropic contributions which can play an important role in the desolvation process. The entropic term is instead considered by the free binding energy method implemented in MD calculations. The latter method was applied by Zacharias and co-workers to calculate the free binding energy of **1** to Gq, starting from the 5CCW X-ray structure [47]. They reported that an absolute binding free energy $\Delta G_{bind,0}$ of -10.4 kcal/mol, in good agreement with the experimental value. ΔE and $\Delta G_{bind,0}$ cannot be quantitatively compared, it is however worth noting that the first is considerably more negative than the latter (-320.8 vs -10.4 kcal/mol).

As mentioned in the preceding Section, this is most probably due to the large PIEs for the electrostatic interaction between two charged fragments, which make the results not quantitatively comparable with the experimental binding energy data [19], whereas the chosen solvent screening model only plays a negligible role in this issue.

An extended PIEs analysis indicated that the large ΔE values can be likely ascribed to the overestimation of the PIEs explicit embedded charge transfer energy for the fragment containing K^+ ion nearest to the ligand. This term, i.e. $\Delta D^{ij} * V^{ij}$ in eq. 3, defines whether surrounding charge distributions of fragments other than i and j promote the charge transfer between i and j in dimer ij [78]. This unusual result might indeed be due to the large number of negatively charged phosphate groups generating an intense negative electrostatic potential field surrounding ligands and K^+ ions overestimating the calculated charge transfer energy. Note that this result is in qualitative agreement with a theoretical work highlighting the relevant contribution of the charge transfer energy in the interaction between DNA Gq and K^+ ions [79].

In this framework, the application of FMO3 or FMO4 approaches might reduce the overestimation of $\Delta D^{ij} * V^{ij}$ terms related to fragments containing K^+ ions in the bound state. **Indeed, as reported in a recent work [80], the “three-body interaction” implemented in FMO3/EDA can correct the overestimation of the charge transfer energy of the FMO2/PIEDA approach. Based on this evidence, part of our future research activities will be devoted to apply the FMO3/EDA with partial solvent screening model to improve the accuracy of the biscarbene-Au(I)/Gq binding energy prediction.**

$\Delta E^{(no K^+)}$ values, on the other hand, are comparable to typical free binding energy values. However, we found negative values for $\Delta E^{(no K^+)}$ only for Gq-1(I), Gq-2(II) and Gq-2(III), whereas one might expect attractive values for all three binding sites and especially for ligand **1** as suggested by the X-Ray structure. Moreover, it is known that K^+ ions play a crucial role in DNA G-q structures [81, 82] and their direct removal would eliminate their effective polarization and charge transfer effects leading to unreliable results. For this reason, we believe that ΔE and F2LE values, although largely overestimating charge transfer energy, can still reliably be used for the ranking of similar metal drugs hitting the same Gq scaffold (receptor), as shown to occur for the substituted naphthalene diimide Gq binders [38].

MD results indicated that the binding pose of **1** in position I undergoes significant fluctuations compared with **1**(II) and **1**(III), since it can adopt three different binding arrangements (B1, B2 and B3) during the simulation [47]. More stable RMSD profiles have instead been reported for **1**(II) and **1**(III). Moreover, the MD study showed that the presence of Au-ligand reduces DNA fluctuation (RMSD and RMSF), especially when all three positions I-III are occupied, yielding to an overall rigidification of the ligand-receptor adduct. [47] We indeed found negative $\Delta E''$ values for DNA bound to **1** or **2**, in position II and III, suggesting that the occupation of these sites can stabilize the Gq fragments structure, in agreement with MD results.

Zacharias and co-workers also estimated the binding energy of ligand **1** in the three positions I-III, by using MD simulations followed by the MM/GBSA method [47]. They reported that the MM/GBSA binding energies for **1**(II) and **1**(III) are more attractive than **1**(I) (Table 4), in contrast to our findings. Such a discrepancy can be ascribed to the marked difference between our FMO-based methodology and the MM/GBSA. We envision that, though the multiconformational MM/GBSA method incorporates the effect of thermal fluctuations relevant to describe the binding at a specific site rather than considering single RL configurations as in FMO2, it is an empirical MM method and cannot take into account quantum mechanical energy components like ligand or fragment polarization, charge transfer, etc., crucial in Gq/biscarbene-Au(I) complex. Indeed, as proposed by Casini and co-workers in the 5CCW X-Ray structure analysis, the Au(I) ion in **1** can be involved in cation- π interactions with the stacking guanines, increasing the binding strength [45]. This was confirmed by Gabbiani and co-

workers who resolved the X-Ray structures of a stable complex between [Au(1-butyl-3-methyl-2-ylidene)₂] and the telomeric Tel23 Gq [46]. In our study, the PIEDA of interaction between ligands and the closest guanine molecules indicates that the most significant attractive energy terms are E^{es} and E^{ct+mix} (Table S2), which are indeed the leading forces of typical metal cation- π interactions [83]. FMO calculations can therefore provide a detailed description and characterization on the nature of chemical bond in LR complex.

The presence of a positively charged metal atom leads to specific interaction properties to the Gq-binder as reported above. A possible improvement of biscarbene-Au(I) Gq-binders could be represented by asymmetric biscarbene-Au(I) ligands, where the Au(I) ion is bound to two different carbene ligands. One carbene should be designed with a polar aromatic scaffold characterized by polar groups to enhance the interaction with the underlying guanine and with K^+ ion, whereas the other ligand should be functionalized so to interact with the remaining G-q regions, as for instance the oligoethylene glycol tail [84]. To this aim, Bonsignore and co-workers synthesized a new series of asymmetric organometallic Au(I)-based Gq binders, characterized by a N-heterocyclic carbene and an alkynyl ligand, which resulted to be selective for the Gq structures but less potent than the lead compound **1** [85]. It is worth noting the new alkynyl-Au(I) compounds are neutral and the absence of a positive charge reduces the interaction with negatively charged phosphate groups and removes the metal π -cation interactions, which play an important role in Au(I) ligand-Gq complex, as indicated by FMO2 results.

As shown here, the FMO method properly describes the non-covalent interactions between Au-ligands and G-q. This type of interactions also occur between Au(I) metal drugs and blood proteins that can act as drug-carrier improving their pharmacokinetics, tumor targeted and in vivo drug delivery [86]. Therefore, the approach described in this paper can be used to characterize such binding and to provide valuable information and help in the design of new biscarbene-Au(I) anticancer drugs with an improved pharmacokinetic profile.

Conclusions

In this work we calculated FMO2 binding energy, ΔE , of two types of biscarbenes Au(I) ligands with DNA Gq. In agreement with the results of FRET-melting assays, we found that ligand **1**, [Au(9-methylcafein-8-ylidene)₂]⁺ binds Gq with a higher affinity than **2**, [Au(1,3-dimethylbenzimidazol-2-ylidene)₂]⁺. Unlike E^{NT} , ΔE includes the deformation-polarization energy and desolvation penalty of both ligand and receptor upon binding. Our results indicate that the deformation-polarization energy of the ligands is the main repulsive term which reduces the ligand binding efficiency. PIEDA also provides an accurate description of the chemical nature of LR interactions indicating that electrostatic and charge-transfer energies are the driving force of the binding process, especially considering the nucleobases and K^+ ion closest to ligands. These findings support the hypothesis that the Au(I) atom can be involved in π -cation interactions with underlying guanine pair that enhance the binding strength of biscarbene-Au(I) ligands. Moreover, the analysis of E_{Li}^{PIE} values suggests that the design of asymmetric ligand, where Au^+ is bound to two different carbene moieties, could be a promising strategy to obtain new potent Au(I)-Gq binders.

It is worth noting that, though FMO2 binding energies can profitably be used for ligand ranking, they can assume very large negative values making the quantitative comparison with experimental binding data difficult.

This is ascribed to the PIEs large values of the K^+ ion containing fragments, overestimating the explicit embedded charge transfer energy in the presence of the ligand. As mentioned above, the use

of the FMO3 or FMO4 approaches might reduce the impact of this issue. Work is in progress to improve the accuracy and the consistency of the FMO binding energy for Gq binders.

The application of the FMO2 procedure shown in this work can be applied in the study of any type of ligand-receptor complex, especially when polarization, dispersion, and charge-transfer interactions play an important role in the binding process.

Supplementary Information The online version contains supplementary material available at..

Data availability The 3D coordinates of Gq, Gq-1₃, Gq-1(I), Gq-1(II), Gq-1(III), Gq-2(I), Gq-1(II), Gq-2(III), ligands 1 and 2 structures reported in this study are also available in the pdb and xyz file formats at the following link <https://doi.org/10.5281/zenodo.7102260> .

Funding No funding was received to assist with the preparation of this manuscript.

Acknowledgements We are thankful to Lorian Storch of the Department of Pharmacy for computer support.

Author contributions Conceptualization: Roberto Paciotti; Formal analysis and investigation: Roberto Paciotti; Writing - original draft preparation: Roberto Paciotti; Writing - review and editing: Cecilia Coletti, Alessandro Marrone, Nazzareno Re, Roberto Paciotti; Supervision: Nazzareno Re. All authors read and approved the final manuscript.

Declarations

Conflict of interest The authors declare that they have no conflict of interest.

References

1. Leelananda SP, Lindert S (2016) Computational methods in drug discovery. *Beilstein J. Org. Chem.* 12: 2694–2718. <https://doi.org/10.3762/bjoc.12.267>
2. Jorgensen WL (2004) The Many Roles of Computation in Drug Discovery. *Science* 303: 1813–1818. <https://doi.org/10.1126/science.1096361>
3. Vanommeslaeghe K, Guvench O, MacKerell Jr DA (2014) Molecular Mechanics *Curr Pharm Des.* 20: 3281–3292.
4. Durrant JD, McCammon JA (2011) Molecular dynamics simulations and drug discovery. *BMC Biology* 9:71. <https://doi.org/10.1186/1741-7007-9-71>
5. Abel R, Wang L, Harder ED, Berne BJ, Friesner RA (2017) Advancing Drug Discovery through Enhanced Free Energy Calculations. *Acc. Chem. Res.* 50:1625–1632. <https://doi.org/10.1021/acs.accounts.7b00083>

- 6.** Meng X, Zhang H, Mezei M, Cui M (2011) Molecular Docking: A powerful approach for structure-based drug discovery *Curr Comput Aided Drug Des.* 7: 146–157. <https://doi.org/10.2174/157340911795677602>
- 7.** Genheden S, Ryde U (2015) The MM/PBSA and MM/GBSA methods to estimate ligand-binding affinities. *Expert Opin. Drug Discov.* 10:449-461. <https://doi.org/10.1517/17460441.2015.1032936>
- 8.** Cole DJ, Horton JT, Nelson L, Kurdekar V (2019) The future of force fields in computer-aided drug design. *Future Med. Chem.* 11:2359–2363. <https://doi.org/10.4155/fmc-2019-0196>
- 9.** Fernández I, Cossío FP (2014) Applied computational chemistry. *Chem. Soc. Rev.* 43: 4906-4908. <https://doi.org/10.1039/C4CS90040E>
- 10.** Krylov A, Windus TL, Barnes T, Marin-Rimoldi E, Nash JA, Pritchard B, Smith DGA, Altarawy D, Saxe P, Clementi C, Crawford TD, Harrison RJ, Jha S, Pande VS, Head-Gordon T (2018) Perspective: Computational chemistry software and its advancement as illustrated through three grand challenge cases for molecular science. *J. Chem. Phys.* 149:180901. <https://doi.org/10.1063/1.5052551>
- 11.** Friesner RA (2005) Ab initio quantum chemistry: Methodology and applications. *PNAS* 102: 6648 – 6653. <https://doi.org/10.1073/pnas.0408036102>
- 12.** Grimme S, Schreiner PR (2018) Computational Chemistry: The Fate of Current Methods and Future Challenges. *Angew. Chem. Int. Ed.* 57:4170 – 4176. <https://doi.org/10.1002/anie.201709943>
- 13.** Friesner RA (2004) Combined quantum and molecular mechanics (QM/MM). *Drug Discovery Today: Technologies* 1:253-260. <https://doi.org/10.1016/j.ddtec.2004.11.008>
- 14.** Fedorov DG, Kitaura K (2007) Extending the Power of Quantum Chemistry to Large Systems with the Fragment Molecular Orbital Method. *J. Phys. Chem. A* 111:6904-6914. <https://doi.org/10.1021/jp0716740>
- 15.** Steinmann C, Fedorov DG, Jensen JH (2010) Effective Fragment Molecular Orbital Method: A Merger of the Effective Fragment Potential and Fragment Molecular Orbital Methods. *J. Phys. Chem. A* 114 (33): 8705–8712. <https://doi.org/10.1021/jp101498m>
- 16.** Fedorov DG, Kitaura K (2006) The three-body fragment molecular orbital method for accurate calculations of large systems. *Chemical Physics Letters* 433:182–187. <https://doi.org/10.1016/j.cplett.2006.10.052>
- 17.** Nakano T, Mochizuki Y, Yamashita K, Watanabe C, Fukuzawa K, Segawa K, Okiyama Y, Tsukamoto T, Tanaka S (2012) Development of the four-body corrected fragment molecular orbital (FMO4) method. *Chemical Physics Letters* 523:128–133. <https://doi.org/10.1016/j.cplett.2011.12.004>
- 18.** Fedorov DG, Kitaura K (2007) Pair Interaction Energy Decomposition Analysis. *J Comput Chem* 28: 222–237. <https://doi.org/10.1002/jcc.20496>
- 19.** Fedorov DG, Kitaura K (2012) Energy Decomposition Analysis in Solution Based on the Fragment Molecular Orbital Method. *J. Phys. Chem. A* 116:704–719. <https://doi.org/10.1021/jp209579w>
- 20.** Ma B, Yamaguchi K, Fukuoka M, Kuwata K (2016) Logical design of anti-prion agents using NAGARA *Biochemical and Biophysical Research Communications* 469:930-935. <https://doi.org/10.1016/j.bbrc.2015.12.106>
- 21.** Paciotti R, Agamennone M, Coletti C, Storchi L (2020) Characterization of PD-L1 binding sites by a combined FMO/GRID-DRY approach. *Journal of Computer-Aided Molecular Design* 34:897–914. <https://doi.org/10.1007/s10822-020-00306-0>
- 22.** Watanabe C, Watanabe H, Fukuzawa K, Parker LJ, Okiyama Y, Yuki H, Yokoyama S, Nakano H, Tanaka S, Honma T (2017) Theoretical Analysis of Activity Cliffs among Benzofuranone-Class Pim1 Inhibitors Using the Fragment Molecular Orbital Method with Molecular Mechanics Poisson–Boltzmann Surface Area (FMO+MMPBSA) Approach. *J. Chem. Inf. Model.* 57:2996–3010. <https://doi.org/10.1021/acs.jcim.7b00110>

23. Heifetz A, Chudyk EI, Gleave L, Aldeghi M, Cherezov V, Fedorov DG, Biggin PC, Bodkin MJ (2016) The Fragment Molecular Orbital Method Reveals New Insight into the Chemical Nature of GPCR–Ligand Interactions. *J. Chem. Inf. Model.* 56:159–172. <https://doi.org/10.1021/acs.jcim.5b00644>
24. Fedorov DG, Kitaura K (2016) Subsystem Analysis for the Fragment Molecular Orbital Method and Its Application to Protein–Ligand Binding in Solution. *J. Phys. Chem. A* 120:2218–2231. <https://doi.org/10.1021/acs.jpca.6b00163>
25. Rhodes D, Lipps HJ (2015) G-quadruplexes and their regulatory roles in biology. *Nucleic Acids Research* 43(18): 8627–8637. <https://doi.org/10.1093/nar/gkv862>
26. Lightfoot HL, Hagen T, Tatum NJ, Hall J (2019) The diverse structural landscape of quadruplexes. *FEBS Letters* 593:2083–2102. <https://doi.org/10.1002/1873-3468.13547>
27. de Luzuriaga IO, Lopez X, Gil A (2021) Learning to Model G-Quadruplexes: Current Methods and Perspectives. *Annu. Rev. Biophys.* 50:209–243. <https://doi.org/10.1146/annurev-biophys-060320-091827>
28. Terenzi A, Bonsignore R, Spinello A, Gentile C, Martorana A, Ducani C, Högberg B, Almerico AM, Lauria A, Barone G (2014) Selective G-quadruplex stabilizers: Schiff-base metal complexes with anticancer activity. *RSC Adv.* 4:33245–33256. <https://doi.org/10.1039/C4RA05355A>
29. Karim NHA, Mendoza O, Shivalingam A, Thompson AJ, Ghosh S, Kuimova MK, Vilar R (2014) Salphen metal complexes as tunable G-quadruplex binders and optical probes. *RSC Adv.* 4: 3355–3363. <https://doi.org/10.1039/C3RA44793F>
30. Keating LR, Szalai VA (2004) Parallel-Stranded Guanine Quadruplex Interactions with a Copper Cationic Porphyrin. *Biochemistry* 43:15891–15900. <https://doi.org/10.1021/bi0483209>
31. Kiełtyka R, Englebienne P, Fakhoury J, Autexier C, Moitessier N, Sleiman HF (2008) A Platinum Supramolecular Square as an Effective G-Quadruplex Binder and Telomerase Inhibitor. *J. Am. Chem. Soc.* 130:10040–10041. <https://doi.org/10.1021/ja8014023>
32. Wu P, Ma DL, Leung CH, Yan SC, Zhu N, Abagyan R, Che C (2009) Stabilization of G-quadruplex DNA with platinum(II) Schiff base complexes: luminescent probe and down-regulation of C-Myc oncogene expression. *Chem. Eur. J.* 15:13008–13021. <https://doi.org/10.1002/chem.200901943>
33. Terenzi A, Lötsch D, van Schoonhoven S, Roller A, Kowol CR, Berger W, Keppler BK, Barone G (2016) Another step toward DNA selective targeting: Ni^{II} and Cu^{II} complexes of a Schiff base ligand able to bind gene promoter G-quadruplexes. *Dalton Trans.* 45:7758–7767. <https://doi.org/10.1039/C6DT00648E>
34. Xia Y, Chen Q, Qin X, Sun D, Zhang J, Liu J (2013) Studies of ruthenium(II)-2,20-bisimidazole complexes on binding to G-quadruplex DNA and inducing apoptosis in HeLa cells. *New J. Chem.* 37:3706–3715. <https://doi.org/10.1039/C3NJ00542A>
35. Chen X, Wu JH, Lai YW, Zhao R, Chao H, Ji LN (2013) Targeting telomeric G-quadruplexes with the ruthenium(II) complexes [Ru(bpy)₂(ptpn)]²⁺ and [Ru(phen)₂(ptpn)]²⁺. *Dalton Trans.* 42:4386–4397. <https://doi.org/10.1039/C3DT32921F>
36. Tuntiwechapikul W, Lee JT, Salazar M (2001) Design and synthesis of the G-quadruplex-specific cleaving reagent perylene-EDTA•iron(II). *J. Am. Chem. Soc.* 123:5606–5607. <https://doi.org/10.1021/ja0156439>
37. Tuntiwechapikul W, Salazar M (2001) Cleavage of telomeric G-quadruplex DNA with perylene-EDTA•Fe(II). *Biochemistry* 40:13652–13658. <https://doi.org/10.1021/bi011363u>
38. Prato G, Silvent S, Saka S, Lamberto M, Kosenkov D (2015) Thermodynamics of Binding of Di- and Tetrasubstituted Naphthalene Diimide Ligands to DNA G-Quadruplex. *J. Phys. Chem. B* 119: 3335–3347. <https://doi.org/10.1021/jp509637y>

39. Neidle S (2017) Quadruplex nucleic acids as targets for anticancer therapeutics. *Nat Rev Chem* 1,0041. <https://doi.org/10.1038/s41570-017-0041>
40. Tassinari M, Cimino-Reale G, Nadai M, Doria F, Butovskaya E, Recagni M, Freccero M, Zaffaroni N, Richter SN, Folini M (2018) Down-regulation of the androgen receptor by G-quadruplex ligands sensitizes castration-resistant prostate cancer cells to enzalutamide. *J. Med. Chem.* 61:8625–8638. <https://doi.org/10.1021/acs.jmedchem.8b00502>
41. Brooks TA, Kendrick S, Hurley L (2010) Making sense of G-quadruplex and i-motif functions in oncogene promoters. *FEBS Journal* 277:3459–3469. <https://doi.org/10.1111/j.1742-4658.2010.07759.x>
42. Lago S, Nadai M, Ruggiero E, Tassinari M, Marušič M, Tosoni B, Frasson I, Cernilogar FM, Pirola V, Doria F, Plavec J, Schotta G, Richter SN (2021) The MDM2 inducible promoter folds into four-tetrad antiparallel G-quadruplexes targetable to fight malignant liposarcoma *Nucleic Acids Research* 49:847–863. <https://doi.org/10.1093/nar/gkaa1273>
43. Bertrand B, Stefan L, Pirrotta M, Monchaud D, Bodio E, Richard P, Le Gendre P, Warmerdam E, de Jager MH, Groothuis GMM, Picquet M, Casini A (2014) Caffeine-Based Gold(I) N-Heterocyclic Carbenes as Possible Anticancer Agents: Synthesis and Biological Properties. *Inorg. Chem.* 53:2296–2303. <https://doi.org/10.1021/ic403011h>
44. Stefan L, Bertrand B, Richard P, Le Gendre P, Denat F, Picquet M, Monchaud D (2012) Assessing the Differential Affinity of Small Molecules for Noncanonical DNA Structures *ChemBioChem* 13:1905-1912. <https://doi.org/10.1002/cbic.201200396>
45. Bazzicalupi C, Ferraroni M, Papi F, Massai L, Bertrand B, Messori L, Gratteri P, Casini A (2016) Determinants for Tight and Selective Binding of a Medicinal Dicarbene Gold(I) Complex to a Telomeric DNA G-Quadruplex: a Joint ESI MS and XRD Investigation. *Angew. Chem.* 128:4328-4331. <https://doi.org/10.1002/ange.201511999>
46. Guarra F, Marzo T, Ferraroni M, Papi F, Bazzicalupi C, Gratteri P, Pescitelli G, Messori L, Biver T, Gabbiani C (2018) Interaction of a gold(I) dicarbene anticancer drug with human telomeric DNA G-quadruplex: solution and computationally aided X-ray diffraction analysis. *Dalton Trans.* 47: 16132-16138. <https://doi.org/10.1039/C8DT03607A>
47. Nays A, Liebl K, Frost CV, Zacharias M (2021) Targeting Telomeres: Molecular Dynamics and Free Energy Simulation of Gold-Carbene Binding to DNA. *Biophysical Journal* 120:101–108. <https://doi.org/10.1016/j.bpj.2020.11.2263>
48. Storchi L, Paciotti R, Re N, Marrone A (2015) Investigation of the molecular similarity in closely related protein systems: The PrP case study. *Proteins* 83:1751–1765. <https://doi.org/10.1002/prot.24836>
49. Paciotti R, Storchi L, Marrone A (2019) An insight of early PrP-E200K aggregation by combined molecular dynamics/fragment molecular orbital approaches. *Proteins* 87:51–61. <https://doi.org/10.1002/prot.25621>
50. Nagase K, Kobayashi H, Yoshikawa E, Kurita N (2009) Ab initio molecular orbital calculations on specific interactions between urokinase-type plasminogen activator and its receptor. *J. Mol. Graph. Model.* 28:46–53. <https://doi.org/10.1016/j.jmgm.2009.04.001>
51. Kurisaki I, Fukuzawa K, Komeiji Y, Mochizuki Y, Nakano T, Imada J, Chmielewski A, Rothstein SM, Watanabe H, Tanaka S (2007) Visualization analysis of inter-fragment interaction energies of CRP–cAMP–DNA complex based on the fragment molecular orbital method. *Biophysical Chemistry* 130:1–9. <https://doi.org/10.1016/j.bpc.2007.06.011>
52. Yoshino R, Yasuo N, Inaoka DK, Hagiwara Y, Ohno K, Orita M, Inoue M, Shiba T, Harada S, Honma T, Balogun EO, da Rocha JR, Montanari CA, Kita K, Sekijima M (2015) Pharmacophore Modeling for Anti-Chagas Drug Design Using the Fragment Molecular Orbital Method. *PLoS ONE* 10(5): 1-15. <https://doi.org/10.1371/journal.pone.0125829>

53. Fedorov DG, Kitaura K, Li H, Jensen JH, Gordon MS (2006) The Polarizable Continuum Model (PCM) Interfaced with the Fragment Molecular Orbital Method (FMO). *J Comput Chem* 27: 976-985. <https://doi.org/10.1002/jcc.20406>
54. Ozawa M, Ozawa T, Ueda K (2017) Application of the fragment molecular orbital method analysis to fragment-based drug discovery of BET (bromodomain and extra-terminal proteins) inhibitors. *J. Mol. Graph. Model.* 74:73–82. <https://doi.org/10.1016/j.jmgm.2017.02.013>
55. Alexeev Y, Mazanetz MP, Ichihara O, Fedorov DG (2012) GAMESS As a Free Quantum-Mechanical Platform for Drug Research. *Current Topics in Medicinal Chemistry* 12:2013-2033. <https://doi.org/10.2174/156802612804910269>
56. Hopkins AL, Keserü GM, Leeson PD, Rees DC, Reynolds CH (2014) The role of ligand efficiency metrics in drug discovery. *Nature Reviews Drug Discovery* 13:105–121. <https://doi.org/10.1038/nrd4163>
57. Abad-Zapatero C (2007) Ligand efficiency indices for effective drug discovery. *Expert Opin. Drug Discov.* 2(4):469-488. <https://doi.org/10.1517/17460441.2.4.469>
58. Mazanetz MP, Ichihara O, Law RJ, Whittaker M (2011) Prediction of cyclin-dependent kinase 2 inhibitor potency using the fragment molecular orbital method. *J Cheminform* 3(2):1-15. <https://doi.org/10.1186/1758-2946-3-2>
59. Otsuka T, Okimoto N, Taiji M (2015) Assessment and Acceleration of Binding Energy Calculations for Protein–Ligand Complexes by the Fragment Molecular Orbital Method. *J. Comput. Chem.* 36:2209–2218. <https://doi.org/10.1002/jcc.24055>
60. Sastry GM, Adzhigirey M, Day T, Annabhimoju R, Sherman W (2013) Protein and ligand preparation: Parameters, protocols, and influence on virtual screening enrichments. *J Comput Aid Mol Des* 27(3):221–234. <https://doi.org/10.1007/s10822-013-9644-8>
61. Schrödinger Release 2018–3: Schrödinger Suite 2018–3 Protein Preparation Wizard; LLC, New York, NY, 2018; Schrödinger Release 2018–3: MacroModel, Schrödinger, LLC, New York, NY, 2018.
62. Frisch, M. J.; Trucks, G. W.; Schlegel, H. B.; Scuseria, G. E.; Robb, M. A.; Cheeseman, J. R.; Scalmani, G.; Barone, V.; Mennucci, B.; Petersson, G. A. Gaussian 09. Revision D.01; Gaussian Inc.: Wallingford, CT, USA, 2009.
63. Bursch M, Neugebauer H, Grimme S (2019) Structure optimisation of large transition-metal complexes with extended tight-binding methods. *Angew. Chem. Int. Ed.* 58:11078-11087. <https://doi.org/10.1002/anie.201904021>
64. Grimme S, Bannwarth C, Shushkov P (2017) A robust and accurate Tight-Binding Quantum Chemical method for structures, vibrational frequencies, and noncovalent interactions of large molecular systems parameterized for all spd-block elements ($Z = 1-86$). *J. Chem. Theory Comput.* 13:1989–2009. <https://doi.org/10.1021/acs.jctc.7b00118>
65. Bannwarth C, Ehlert S, Grimme S (2019) GFN2-xTB-An accurate and broadly parametrized self-consistent Tight-Binding Quantum Chemical method with Multipole Electrostatics and Density-Dependent Dispersion contributions. *J. Chem. Theory Comput.* 15: 1652–1671. <https://doi.org/10.1021/acs.jctc.8b01176>
66. Ishikawa T, Kuwata K (2012) RI-MP2 Gradient Calculation of Large Molecules Using the Fragment Molecular Orbital Method *J. Phys. Chem. Lett.* 3: 375–379. <https://doi.org/10.1021/jz201697x>
67. Ishikawa T, Kuwata K (2009) Fragment molecular orbital calculation using the RI-MP2 method. *Chemical Physics Letters* 474: 195–198. <https://doi.org/10.1016/j.cplett.2009.04.045>

- 68.** Rahalkar AP, Katouda M, Gadre SR, Nagase S (2010) Molecular Tailoring Approach in Conjunction with MP2 and RI-MP2 Codes: A Comparison with Fragment Molecular Orbital Method. *J. Comput. Chem.* 31: 2405–2418. <https://doi.org/10.1002/jcc.21533>
- 69.** Pham BQ, Gordon MS (2020) Development of the FMO/RI-MP2 Fully Analytic Gradient Using a Hybrid-Distributed/Shared Memory Programming Model. *J. Chem. Theory Comput.* 16:1039–1054. <https://doi.org/10.1021/acs.jctc.9b01082>
- 70.** Floris FM, Tomasi J, Ahuir JP (1991) Dispersion and repulsion contributions to the solvation energy: refinements to a simple computational model in the continuum approximation. *J. Comput. Chem.* 12:784-791. <https://doi.org/10.1002/jcc.540120703>
- 71.** Si D, Li H (2009) Heterogeneous conductor like solvation model. *J. Chem. Phys.* 131, 044123. <https://doi.org/10.1063/1.3187527>
- 72.** Pierotti RA (1976) A scaled Particle Theory of Aqueous and Nonaqueous Solutions. *Chem. Rev.* 76:717–726.
- 73.** Langlet J, Claverie P, Caillet J, Pullman A (1988) Improvements of the continuum model. 1. Application to the calculation of the vaporization thermodynamic quantities of nonassociated liquids. *J. Phys. Chem.* 92:1617–1163. <https://doi.org/10.1021/j100317a048>
- 74.** Mori H, Ueno-Noto K, Osanai Y, Noro T, Fujiwara T, Klobukowski M, Miyoshi E (2009) Revised model core potentials for third-row transition–metal atoms from Lu to Hg. *Chem. Phys. Lett.* 476:317–322. <https://doi.org/10.1016/j.cplett.2009.06.019>
- 75.** Barca GMJ, Bertoni C, Carrington L, Datta D, De Silva N, Deustua JE, Fedorov DG, Gour JR, Gunina AO, Guidez E, Harville T, Irlé S, Ivanić J, Kowalski K, Leang SS, Li H, Li W, Lutz JJ, Magoulas I, Mato J, Mironov V, Nakata H, Pham BQ, Piecuch P, Poole D, Pruitt SR, Rendell AP, Roskopf LB, Ruedenberg K, Sattasathuchana T, Schmidt MW, Shen J, Slipchenko L, Sosonkina M, Sundriyal V, Tiwari A, Vallejo JLG, Westheimer B, Włoch M, Xu P, Zahariev F, Gordon MS (2020) Recent developments in the general atomic and molecular electronic structure system. *J. Chem. Phys.* 152:154102. <https://doi.org/10.1063/5.0005188> Versions “5 DEC 2014 - R1” and “30 JUN 2021 - R1”.
- 76.** Okiyama Y, Nakano T, Watanabe C, Fukuzawa K, Mochizuki Y, Tanaka S (2018) Fragment Molecular Orbital Calculations with Implicit Solvent Based on the Poisson–Boltzmann Equation: Implementation and DNA Study. *J. Phys. Chem. B* 122:4457–4471. <https://doi.org/10.1021/acs.jpcc.8b01172>
- 77.** Fedorov DG (2019) Solvent Screening in Zwitterions Analyzed with the Fragment Molecular Orbital Method. *J. Chem. Theory Comput.* 15: 5404–5416. <https://doi.org/10.1021/acs.jctc.9b00715>
- 78.** Fedorov DG, Asada N, Nakanishi I, Kitaura K (2014) The Use of Many-Body Expansions and Geometry Optimizations in Fragment-Based Methods. *Acc. Chem. Res.* 47:2846–2856. <https://doi.org/10.1021/ar500224r>
- 79.** Yurenko YP, Novotný J, Sklenář V, Marek R (2014) Exploring non-covalent interactions in guanine and xanthine-based model DNA quadruplex structures: a comprehensive quantum chemical approach. *Phys. Chem. Chem. Phys.* 16:2072-2084. <https://doi.org/10.1039/C3CP53875C>
- 80.** Fedorov DG (2020) Three-Body Energy Decomposition Analysis Based on the Fragment Molecular Orbital Method. *J. Phys. Chem. A* 124: 4956–4971. <https://doi.org/10.1021/acs.jpca.0c03085>
- 81.** Lightfoot HL, Hagen T, Tatum NJ, Hall J (2019) The diverse structural landscape of quadruplexes. *FEBS Letters* 593:2083–2102. <https://doi.org/10.1002/1873-3468.13547>
- 82.** Zaccaria F, Paragi G, Fonseca Guerra C (2016) The role of alkali metal cations in the stabilization of guanine quadruplexes: why K^+ is the best. *Phys. Chem. Chem. Phys.* 18:20895-20904. <https://doi.org/10.1039/C6CP01030J>

- 83.** Mecozzi S, West AP, Dougherty DA (1996) Cation- π Interactions in Simple Aromatics: Electrostatics Provide a Predictive Tool. *J. Am. Chem. Soc.* 118:2307-2308. <https://doi.org/10.1021/ja9539608>
- 84.** Tateishi-Karimata H, Ohyama T, Muraoka T, Podbevsek P, Wawro AM, Tanaka S, Nakano S, Kinbara K, Plavec J, Sugimoto N (2017) Newly characterized interaction stabilizes DNA structure: oligoethylene glycols stabilize G-quadruplexes CH- π interactions. *Nucleic Acids Res.* 45: 7021–7030. <https://doi.org/10.1093/nar/gkx299>
- 85.** Meier-Menches SM, Aikman B, Döllner D, Klooster WT, Coles SJ, Santi N, Luk L, Casini A, Bonsignore R (2020) Comparative biological evaluation and G-quadruplex interaction studies of two new families of organometallic gold(I) complexes featuring N-heterocyclic carbene and alkynyl ligands. *J. Inorg. Biochem.* 202(110844):1-12. <https://doi.org/10.1016/j.jinorgbio.2019.110844>
- 86.** Sen S, Perrin MW, Sedgwick AC, Lynch VM, Sessler JL, Arambula JF (2021) Covalent and non-covalent albumin binding of Au(I) bis-NHCs via post-synthetic amide modification. *Chem. Sci.* 12:7547–7553. <https://doi.org/10.1039/D1SC01055G>